Nanostructure Characterization of Co-Pd-Si-O Soft Magnetic Nanogranular Film using Small-Angle X-ray and Neutron Scattering

Yojiro Oba[1,a),b)], Masato Ohnuma[1], Shigehiro Ohnuma[2], Michihiro Furusaka[3], Suresh Koppoju[1], Shin Takeda[3]

[1]*National Institute for Materials Science, Tsukuba, Ibaraki 305-0047, Japan*
[2]*Research Institute for Electromagnetic Materials, Sendai, Miyagi 982-0807, Japan*
[3]*Hokkaido University, Sapporo, Hokkaido 060-8628, Japan*

The nanostructure of a Co-Pd-Si-O nanogranular film was investigated with the combined use of small-angle x-ray (SAXS) and neutron scattering (SANS). Using a new, compact type of SANS instrument, the SANS profiles of individual particles with a diameter of about 2-4 nm were successfully observed. The structures of magnetic regions were found to be the same as the chemical structures of the particles, and a sharp interface was observed between the matrix and the particles. The SAXS to SANS ratio clearly indicates that the particles are a CoPd alloy and the matrix is not pure SiO_2. In fact, the matrix is composed of a meaningful amount of Co.

KEYWORDS: small-angle x-ray scattering; small-angle neutron scattering; nanogranular film; Co; soft magnetic material

1. INTRODUCTION

Nanogranular films composed of magnetic metal particles embedded in an oxide, nitride, or fluoride matrix attract a lot of attention in the field of magnetic materials [1-5]. These advanced soft magnetic materials are potential for the high frequency applications [4-6]. Cobalt oxide nanogranular films, such as Co-Al-O or Co-Zr-O, are suitable candidates at the GHz range, because they simultaneously have a high magnetic anisotropy, high electrical resistivity, and high saturation magnetic flux density. Ohnuma *et. al.* reported that the soft magnetic property, especially magnetic anisotropy, enhanced with an addition of Pd to the Co-Si-O nanogranular films [6]. However, the origins of the enhanced magnetic anisotropy and the effect of the Pd are still controversial due to a lack of morphological information

a) Electronic mail: oba@rri.kyoto-u.ac.jp
b) Present address: *Research Reactor Institute, Kyoto University, Kumatori-cho, Osaka 590-0494, Japan*

about the magnetic particles. In order to resolve those issues and obtain optimal soft magnetic properties, knowledge of the nanostructure of the film is required. In previous studies of nanogranular films, a possible intermixing of magnetic elements into the amorphous matrix was often noted [7-10]. A magnetic element dispersed in the matrix can influence the magnetic properties via a reduction of magnetization, a modulation of magnetic coupling, and/or a change in transport properties [11]. However, it is difficult to evaluate the partition between the particles and the matrix using traditional experimental methods such as an energy dispersive x-ray spectroscopy using transmission electron microscope (TEM-EDX) or three dimensional atom probe field ion microscopy (3D-APFIM). Although such methods are powerful tools for the direct observation of nanostructures in great detail, for particles only a few nm in diameter embedded in the matrix, the matrix effects overlapping signals from the particles are inevitable. X-ray spectroscopic methods, such as x-ray absorption fine structure spectroscopy (XAFS) and x-ray photoemission spectroscopy (XPS) are also useful techniques because they enable analysis of the chemical states of the magnetic elements. However, they provide little information about structures.

Small-angle scattering (SAS) is a suitable means for nanostructure investigation. While the structural information obtained from SAS is not straightforward due to reciprocal space analysis, compared with TEM and 3D-APFIM, SAS has a great advantage in observable volume and statistical accuracy [12,13]. Prior nanogranular film work has demonstrated the potential of small-angle x-ray scattering (SAXS) and neutron scattering (SANS) for nanostructure investigation [14-18]. Furthermore, recent studies have reported that the combined use of SAXS and SANS can provide information concerning the chemical composition of the particles separate from that of the matrix [13,19]. This new technique is named as the *alloy contrast variation* (ACV) method. The magnetic scattering contribution from SANS also enables the analysis of magnetic structures, which is one of the most critical pieces of information in the characterization of magnetic materials [20-24]. To date, applications of the SANS and ACV methods have been quite limited because conventional SANS instruments are optimized for the measurement of the q region below ~1 nm^{-1}, in which scattering from structures larger than $2\pi/1 = 6$ nm is observable. Here q is a momentum transfer and equal to $4\pi\sin\theta/\lambda$, where λ is the wavelength of the incident radiation and θ is half the scattering angle. However, for nanosized materials composed of 2-3 nanometer features, a higher q region is essential. Recently, with the advent of advanced neutron optics techniques, a state-of-the-art *mini-focusing SANS* (*mf-SANS*)

instrument was developed at research reactor JRR-3 in Japan [25]. It proved that a SANS instrument, even with a low neutron beam intensity and compact size, can operate properly. In particular, its compact size is suitable for the measurement in high q region. Thus, the study of precise nanoscale structures using the SAXS, SANS, and ACV methods is now possible.

In this study, SAXS and SANS techniques were used to study the nano- and magnetic structures of the Co-Pd-Si-O nanogranular films and ACV method was applied to obtain their chemical structure. The formation of magnetic particles, the partitioning states of the Co and Pd, and the effects of the Pd on the magnetic properties are discussed.

2. EXPERIMENTAL PROCEDURE

Samples of Co-Pd-Si-O nanogranular films were prepared by the radio frequency (RF) reactive magnetron sputtering method in Ar-O_2 gas. A Co-Si alloy disk target was used for the sputtering of the films and Pd chips were placed on top of the target. 2 μm thick films were deposited on 0.5 mm thick single crystal Si substrates. Details of the preparation can be found elsewhere [6]. The chemical composition of the samples was determined using Rutherford back scattering (RBS) spectrometry. The measured chemical composition of the film is $Co_{59}Pd_{11}Si_8O_{22}$. Magnetic measurements were performed using a vibrating sample magnetometer (VSM).

A typical SAXS instrument using Cu as the x-ray source is not suitable for this study because Cu $K\alpha$ x-rays are strongly absorbed by Co, resulting in x-ray fluorescence which causes a high background. Therefore, the SAXS measurements were performed using a SAXS instrument with Mo $K\alpha$ radiation (RIGAKU, Nano-viewer) and a two-dimensional detector (PILATUS-100k) at the National Institute for Materials Science (NIMS) in Japan. Furthermore, in transmission geometry, Mo $K\alpha$ x-rays also have an advantage in that they penetrate through the Si substrates due to their high energy. The incident x-ray was focused using a two-dimensional confocal mirror and collimated using the pinhole technique. The beam diameter at the sample was ~0.5 mm. The distance between the samples and the detector was 1.06 m, which covers q range from 0.2 to 5 nm^{-1}. In order to obtain the SAXS profile only from the nanogranular film, the profiles of virgin Si substrate was measured and subtracted from the SAXS profiles obtained from the films with Si substrate.

SANS measurements generally require a larger amount of sample compared to SAXS

measurements. Hence, 26 nanogranular films were stacked to obtain a SANS sample of sufficient thickness (tens of μm) to obtain acceptable statistical accuracy. The dimensions of each film were ~20 mm high × ~20 mm wide × 2 μm thick. SANS measurements were carried out using the mf-SANS installed in the JRR-3 research reactor at the Japan Atomic Energy Agency [25]. The detector was an array of 48 one-dimensional ^{3}He position-sensitive detectors (PSD). The diameter and length of each PSD were 1.27 mm and 600 mm, respectively. The distance between the samples and the detector was 0.6 m. Stacked, bent Si slabs were used as a high efficiency monochrometer. The wavelength was 0.58 nm. To saturate the magnetization and align the magnetic scattering contribution, a magnetic field of 0.5 T was applied parallel to the sample plane using a Halbach-type permanent magnet. The SANS intensity perpendicular to the magnetic field is composed of the magnetic scattering as well as the nuclear scattering.

For conversion of both the SAXS and SANS intensity to absolute scattering intensity, glassy carbon characterized at the Argonne National Laboratory was used as a standard [26].

3. RESULTS AND DISCUSSION

Fig. 1 shows the two-dimensional (2D) SAXS pattern of the $Co_{59}Pd_{11}Si_8O_{22}$ nanogranular film. The dark spot around q=0 is caused by a direct beam stop and is not an intrinsic property of the sample. The clear ring observed at q=1-2 nm^{-1} is a typical feature of the interparticle interference effect which indicates that the particles are present and are densely packed in the film [27]. The SAXS intensity has no anisotropic pattern across the entire observable range. Fig. 2 shows azimuthal plots obtained from Fig.1 in several q regions of 0.8-0.9, 1.5-1.6, and 3.0-3.1 nm^{-1}. The horizontal axis is the azimuth angle β in the 2D detector plane. It can be seen from the Fig. 2 that β dependences are completely flat. This clearly demonstrates that the nanostructures are isotropic. Therefore, it is concluded that the orientation of the particle is random, and any shape anisotropy of the particles does not contribute to the magnetic anisotropy of the film.

The q-dependence of the SAXS intensity $I_{SAXS}(q)$ in absolute units converted from Fig. 1 is shown in Fig. 3. Although the q range available under the present measurement conditions is between 0.15 and 4.5 nm^{-1}, the SAXS intensity of the sample in the q<0.4 nm^{-1} is missing due to very low scattering from the sample. The profile exhibits a clear peak at q=1.5 nm^{-1} and then decreases in proportion to q^{-4} in the higher q region. These features correspond to

the scattering of densely packed spherical particles [27]. A similar peak was reported in previous studies of several other nanogranular films prepared using the sputtering method [14-18].

For further analysis of the nanostructures, a curve fitting was carried out. In a system including densely packed particles, the interference effect from the x-ray or neutrons scattered from the particles has to be taken into account. When the particles have a size distribution, the *local monodisperse approximation* is useful to involve polydispersity into the interparticle interference effect [28]. This approximation assumes that the particles are locally monodispersed and is written as,

$$I_i(q) = d_N \Delta\rho_i^{\,2} \int_0^\infty V_i^2 F_i^2(q,r) N_i(r) S_i(q,r) dr, \qquad (1)$$

where d_N and $\Delta\rho$ are the number density of particles and the excess scattering length density, respectively. These values are independent of q. The parameters r and V are the radius and volume of the particles. $F(q,r)$, $N(r)$, and $S(q,r)$ describe the form factor (which is determined from particle shape), the size distribution function, and the structure factor (which represents the interparticle interference effect). The subscript i is either *SAXS* or *SANS*, depending on the technique in use. Based on TEM observations and the orientation discussion above, the shape of the particle in the nanogranular sample is regarded as spherical, for which $F(q,r)$ and V are given by,

$$F(q,r) = 3\frac{\sin(qr) - qr\cos(qr)}{(qr)^3}, \text{ and} \qquad (2)$$

$$V = \frac{4}{3}\pi r^3. \qquad (3)$$

The Percus-Yevick approximation with a hard-sphere potential was selected for $S(q)$ [27]. It involves the volume fraction of the particles V_{hs} and the interaction radius r_{hs}. For $N(r)$, a logarithmic-normal distribution function is typically assumed. It is represented as,

$$N(r) = \frac{1}{\sqrt{2\pi}wr}\exp\left\{-\frac{(\ln r - \ln r_m)^2}{2w^2}\right\}, \qquad (4)$$

where r_m and w are the median and logarithmic standard deviations, respectively. Using these parameters, the average D_{ave} and standard deviation σ of the diameter are expressed as,

$$D_{ave} = 2r_m \exp(w^2/2), \text{ and} \quad (5)$$

$$\sigma = 2r_m \sqrt{\exp(w^2)\{\exp(w^2)-1\}}\,. \quad (6)$$

However, for the present nanogranular films, a simple lognormal function cannot be used to interpret the experimental SAXS profiles, because the shoulder at q~3 nm^{-1} is a typical feature of narrow size distribution, whereas the peak shape broadened in the low q region indicates a wide size distribution. This suggests that the sample is composed of at least two types of particles: particles with a narrow size distribution, and particles with a wide size distribution. Thus, a summation of two lognormal functions $N(r) = N_A(r) + N_B(r)$, where suffixes A and B denote individual particles defined by each average D_A or D_B and standard deviation σ_A or σ_B, was used for fitting.

Figure 3 also shows the fitted curve. It agrees well with the experimental results. This is the first experimental result for these two particle components. The parameters obtained from the fitting are summarized in Table 1. While particles A and B have narrow and wide size distributions, respectively, the D_A is larger than the D_B. The A particles probably correspond to the primary particles previously observed via TEM because a sharp size distribution has usually been obtained in nanogranular films prepared using the sputtering method [6,14]. The existence of B particles provide possible effects of a surface and an interface between the substrate and the film. In previous studies, anomalous segregation and growth of Co particles in silica matrix around surface or interface have often been reported [29-31]. Another review also pointed out that those segregation and particle growth result in the broadening of size and shape distributions [32]. Therefore, the B particles observed in the present study possibly correspond to the particles affected by the surface and interface.

Next, the SANS results were analyzed. The SANS intensity is separated into two components: nuclear $I_{nuc}(q)$ and magnetic scattering contributions $I_{mag}(q)$ [20]. While the former is the scattering from nuclei and gives information about the chemical structures, the latter is scattering due to the magnetic moment and provides the magnetic structures. Magnetic scattering occurs only in the direction perpendicular to q and the magnetic moment m. $I_{nuc}(q)$ is regarded as isotropic because both $I_{SAXS}(q)$ and $I_{nuc}(q)$ reflect information about

the chemical structures of identical samples. In the saturated magnetization state attained by applying a uniform magnetic field, the total SANS intensity $I_{SANS}(q)$ is expressed as [20],

$$I_{SANS}(q) = I_{nuc}(q) + I_{mag}(q)\sin^2\alpha, \qquad (7)$$

where α is the angle between q and m on the detector plane. A magnetic field of 5000 Oe is sufficient to saturate the magnetization [5,6]. Therefore, the contribution parallel to the magnetic field $I_{//}$ and perpendicular to the magnetic field $I_{\perp}$ are given by,

$$I_{//}(q) = I_{nuc}(q), \text{ and} \qquad (8)$$

$$I_{\perp}(q) = I_{nuc}(q) + I_{mag}(q). \qquad (9)$$

The q-dependent SANS intensity $I_{//}(q)$ and $I_{\perp}(q)$ of the sample are shown in Fig. 4. Sector averages were taken at sector angles of ±15 degrees with respect to a=0^o and 90^o for $I_{//}(q)$ and $I_{\perp}(q)$. The noisy $I_{//}(q)$ indicates that nuclear scattering is weak. This is attributed to the low contrast of $\Delta\rho_{nuc}$ between the particle and the matrix. In the low q region of $I_{//}(q)$, there is no valid data point due to weak intensity of $I_{//}(q)$ and the lack of effective detector pixel. On the other hand, the $I_{\perp}(q)$ shows significant scattering, and its shape is very similar to $I_{SAXS}(q)$. Because of the low $I_{nuc}(q)$, the $I_{\perp}(q)$ is regarded as primarily a contribution from the $I_{mag}(q)$. This implies that the magnetic regions in the sample have similar structures, including the shape and size of the particles. The simplest explanation of this result is that the particles and the matrix correspond to the magnetic and nonmagnetic regions, respectively. As a result, it is concluded that the magnetization in the particles is uniform and the magnetic particles have a clear interface between the particle and the matrix. There is no apparent interface layer, such as an oxide layer.

Subsequently, a combined analysis using both the SAXS and SANS results was performed. All of the SAS profiles $I_{SAXS}(q)$, $I_{nuc}(q)$ and $I_{mag}(q)$ are basically expressed by eq. (1). The ACV method analyzes the ratio of $I_{SAXS}(q)$ and $I_{nuc}(q)$. Since the V_{SAXS}, $F_{SAXS}(q,r)$, $N_{SAXS}(r)$, and $S_{SAXS}(q,r)$ are essentially identical to those from nuclear scattering, the ratio of the SAXS to SANS profiles only gives the ratio of square scattering length density $\Delta\rho_{SAXS}^2/\Delta\rho_{nuc}^2$, which includes nanostructure chemical composition information [13,19]. The other terms in eq. (1), including information about the shape and size of the particles, cancel.

Unfortunately, for the present Co-Pd-Si-O nanogranular films, application of the normal ACV method is difficult due to its poor $I_{nuc}(q)$ statistics. However, the present sample shows clear magnetic scattering and $I_{\perp}(q)$ is accurate. This is also useful because the above discussion details that the structure of the magnetic regions in the present sample is almost same as the structure of the particles. This provides that the V_{mag}, $F_{mag}(q,r)$, $N_{mag}(r)$, and $S_{mag}(q,r)$ in eq. (1) are also equal to those due to nuclear scattering and x-rays. Several research groups have previously reported the combined use of $I_{mag}(q)$ and $I_{nuc}(q)$ [33-36]. In this study, the ratio of $I_{SAXS}(q)$ to $I_{\perp}(q)$ is analyzed instead of $I_{nuc}(q)$. Because of the low accuracy of $I_{nuc}(q)$, the extraction of $I_{mag}(q)$ from $I_{\perp}(q)$ causes a large error for $I_{mag}(q)$ based on eq. (9). In the present case, the ratio $I_{SAXS}(q)/I_{\perp}(q)$ corresponds to $\Delta\rho_r^2=\Delta\rho_{SAXS}^2/(\Delta\rho_{nuc}^2+\Delta\rho_{mag}^2)$. Since the magnitude of ρ_{mag} is proportional to the magnetization, the ratio $\Delta\rho_r^2$ can be calculated if reference data for magnetization is available. Therefore, the chemical composition can be determined from a comparison of the experimental ratio $I_{SAXS}(q)/I_{\perp}(q)$ with the calculated ratio $\Delta\rho_r^2$.

Fig. 5 shows the $I_{SAXS}(q)/I_{\perp}(q)$ profile evaluated using the data from Figs. 3 and 4. The plots are almost constant in the q range higher than 1.2 nm^{-1}. The highest q range (> 2.5 nm^{-1}) is not considered in the present discussion because of excessively large error. The q range between 1.2 and 2.5 nm^{-1} agrees with the peak observed in both $I_{SAXS}(q)$ and $I_{\perp}(q)$. The good statistics in this q range are attributed to the high scattering intensity around the peak. This constant ratio confirms that the chemical composition is uniform throughout the particles. The average value of the experimental ratio $I_{SAXS}(q)/I_{\perp}(q)$ between q = 1.2 and 2.5 nm^{-1} is 120, which is shown in Fig. 5 as a horizontal dotted line. In the q range lower than 1.2 nm^{-1}, the ratio gradually decreases. Since the validity of both SAXS and SANS profiles in this q region was confirmed by the measurements of the standard (glassy carbon), this decrease is significant and indicates the presence of structure larger than individual particle. This is possibly due to a higher order magnetic structure, such as magnetic domains expanding over several particles. However, the present SANS results have resolution too low for further analysis.

Then, the $\Delta\rho_r^2$ ratio was calculated using reference data. The first candidate for this sample was Co-Pd particles in a Si-O matrix. There is a lot of magnetic data available for bulk Co-Pd, as well as the crystal structure, because Co-Pd is a well-known magnetic material in which Co induces a magnetic moment in Pd. Many studies about magnetic properties of Co-Pd have been carried out [37-39]. Since Si-O is also a popular material,

there is similarly a large amount of data [40,41]. Using those references, $\Delta\rho_r^2$ values were calculated assuming that the samples consist of Co_xPd_{1-x} particles embedded in SiO_2 (Fig. 6). It was first assumed that the Co was perfectly separated from the matrix. Since a sector angle of ±15 degrees for the sector average of $I_\perp(q)$ reduces the magnitude of $I_{mag}(q)$ to 98% as is obvious from eq. (7), the calculated $\Delta\rho_r^2$ includes 98% of $\Delta\rho_{mag}^2$. The experimental value evaluated from the $I_{SAXS}(q)/I_\perp(q)$ ratio is also shown in Fig. 6 as a dotted line. The value of x is 0.84 in the present chemical composition, $Co_{59}Pd_{11}$. The calculated $\Delta\rho_r^2$ is higher than the experimental value of 120 over all x. This indicates that the sample is not pure Co_xPd_{1-x} particles and a SiO_2 matrix system.

The results of the magnetic measurements also support this deviation from a pure Co_xPd_{1-x}/SiO_2 system. Figure 7 shows the magnetic hysteresis loops along the magnetization easy and hard axes of the present sample. The magnetizations of the easy and hard axes are saturated at ~100 and ~400 Oe, respectively. The large deference of about 300 Oe between the easy and hard axes loops indicates the large magnetic anisotropy in the sample. The saturation magnetization $4\pi M_s$ of the present sample is 8.4 kG. The value obtained is 55% of that of bulk $Co_{0.84}Pd_{0.16}$. If a completely separated Co_xPd_{1-x}/SiO_2 system is assumed and their mass densities are used, the volume fraction of the $Co_{0.84}Pd_{0.16}$ particles is estimated to be 66%. The present experimental result is only 84% of the ideal Co_xPd_{1-x}/SiO_2 state. Since the magnetization depends only on the magnetic moment of Co or Pd and the volume of the sample, this indicates that the magnetic moments and/or mass density of the sample become smaller than those of the bulk crystal.

Then, the possible effects of this decrease in the magnetization of the Co_xPd_{1-x} particles were considered, because it is usual for magnetic particles to experience such phenomena as surface oxidation and size effects. However, such a decrease in the magnetization raises the calculated values of $\Delta\rho_r^2$ and makes the gap between the calculations and experiments wider. In contrast, an increase in the magnetization reduces the calculated $\Delta\rho_r^2$, but this is inconsistent with the magnetic measurements and is generally not accepted for typical magnetic materials. Furthermore, the effect of a change in the mass density of the SiO_2 matrix was also evaluated. However, this alteration has a minimal impact on the calculated $\Delta\rho_r^2$ because $\Delta\rho_{SAXS}^2$ is dominated by the ρ_{SAXS} of the particles, and the contribution of the SiO_2 matrix to $\Delta\rho_{SAXS}^2$ is small. In addition, the contribution of $\Delta\rho_{nuc}^2$ to the calculated $\Delta\rho_r^2$ is also small. Hence, the first assumption that the no Co exists in the matrix is probably not appropriate for the present sample. The values of $\Delta\rho_r^2$ for the Co_xPd_{1-x} particles/Co-Si-O

matrix system were then calculated. Oxidized Co is known to have no magnetic ordering at room temperature and antiferromagnetic ordering at low temperature [42,43]. This is consistent with the results of the magnetic measurements which show the decrease in the magnetization. Since Pd is a noble metal and is difficult to oxidize, possible intermixing of Pd into the matrix is excluded. As a reference for the Co-Si-O matrix, the values of $\Delta\rho_r^2$ for cobalt silicate Co_2SiO_4 and cobalt oxide CoO were calculated [44-46]. The calculated $\Delta\rho_r^2$ for these matrices are lower than the experimental values (Fig. 8). This indicates that Co in the matrix decreases the value of $\Delta\rho_r^2$. Compared to the pure Co_xPd_{1-x}/SiO_2 system, it can be concluded that the chemical composition of the present sample is primarily Co_xPd_{1-x}/SiO_2, and that the Co is partially dispersed into the matrix. Based on this model, the amount of Co in the matrix can be roughly estimated. CoO and SiO_2 were selected as calculation models for the matrix. Figure 9 shows the value of $\Delta\rho_r^2$ in the system of $Co_{59-y}Pd_{11}/(CoO)_y(SiO_2)_8$ calculated using crystallographic data from CoO and SiO_2. The experimental $\Delta\rho_r^2$ coincides with the value calculated for y=3 at.%. This corresponds to $Co_{0.84}Pd_{0.16}$ and $Co_{0.09}Si_{0.24}O_{0.67}$. The ratio of Co in the matrix to the total amount is 5%. This indicates that a significant, but not large, amount of Co is dispersed in the matrix and oxidized. The calculated value of $\Delta\rho_{nuc}^2$ for this chemical composition is about 25 % of $\Delta\rho_{mag}^2$. With increasing Co in the matrix, the value of $\Delta\rho_{nuc}^2$ also increases, but it is still smaller than $\Delta\rho_{mag}^2$. This coincides with the low accuracy of $I_{nuc}(q)$.

In Co-Pd alloy films and multilayers, Pd is known to significantly enhance the magnetic anisotropy via crystallographic effects like magnetostriction or spin-orbit coupling of its large orbital magnetic moment [47-4]. Therefore, in the present Co-Pd-Si-O nanogranular films, the large magnetic anisotropy field can probably be attributed to the crystallographic magnetic anisotropy of the Co-Pd alloy.

4. CONCLUSION

Nanostructure of the $Co_{59}Pd_{11}Si_8O_{22}$ nanogranular film has been reported using SAXS and the SANS. Using mf-SANS, significant scattering from particles with a diameter less than 4 nm was observed. First, the SAXS pattern indicates that the nanostructure of the nanogranular film is isotropic. Second, the particles are composed of two components. One has a narrow size distribution with larger average diameter and probably corresponds to the primary portion of the film. The other has a wider size distribution with smaller average diameter. Finally, from an analysis of the $\Delta\rho_r^2$ ratio, the chemical composition of the

particles was found to be CoPd and it was detected that small fraction of Co was dissolved into the matrix. Co was also detected dissolved the matrix. Using SAS and ACV techniques, the particle/matrix partition in a nanogranular film has been quantitatively investigated for the first time. The information provided by this work will stimulate further nanogranular film research and development.

ACKNOWLEDGEMENTS

The authors thank Mr. T. Miyata in Hokkaido University and Mr. Y. Nishikawa and Prof. M. Sugiyama in Kyoto University for their help with the SANS experiments and Mr. P. Kozikowski in Warsaw University of Technology for fruitful discussion. This work was supported by a JSPS KAKENHI Grant Number 22604003 and Quantum Beam Technology Program of The Ministry of Education, Culture, Sports, Science and Technology.

REFERENCES

[1] J. Q. Xiao, J. S. Jiang, and C. L. Chien, Phys. Rev. Lett 68 (1992) 3749-3752.

[2] C. T. Black, C. B. Murray, R. L. Sandstrom, S. Sun, Science 290 (2000) 1131-1134.

[3] T. Oikawa, M. Nakamura, H. Uwazumi, T. Shimatsu, H. Muraoka, and Y. Nakamura, IEEE Trans. Magn. 38 (2002) 1976-1978.

[4] K. Hono and M. Ohnuma, Microstructures and Properties of Nanocrystalline and Nanogranular Magnetic Materials, in: H. S. Nalwa, Magnetic Nanostructures, American Scientific Publishers, California, 2002, pp. 327-358.

[5] S. Ohnuma, N. Kobayashi, H. Fujimori, and T. Masumoto, J. Phys. Conf. Ser. 191 (2009) 012020/1-6.

[6] S. Ohnuma, N. Kobayashi, T. Masumoto, S. Mitani, and H. Fujimori, J. Magn. Soc. Japan 23 (1999) 240-242.

[7] H. Kumar, S. Ghosh, D. Bürger, L. Li, S. Zhou, D. Kabiraj, D. K. Avasthi, R. Grötzschel, and H. Schmidt, J. Appl. Phys. 109 (2011) 073914/1-9.

[8] G. I. Frolov, V. S. Zhigalow, S. M. Zharkov, A. I. Pol'skii, and V. V. Kirgizov, Phys. Solid State 45 (2003) 2303-2308.

[9] R. Kondo, K. Ikeda, K. Kobayashi, and M. Fujimoto, J. Ceram. Soc. Jpn. 110 (2002) 614-617.

[10] K. Asami, S. Mitani, H. Fujimori, S. Ohnuma, and T. Masumoto, Surf. Interface Anal. 28 (1999) 250-253.

[11] F. Guinea, Phys. Rev. B 58 (1998) 9212-9216.

[12] S. Ohtsuka, T. Kaito, S. Kim, M. Inoue, T. Asayama, M. Ohnuma, and J. Suzuki, Mater. Trans. 50 (2009) 1778-1784.

[13] M. Ohnuma, J. Suzuki, S. Ohtsuka, S.-W. Kim, T. Kaito, M. Inoue, and H. Kitazawa, Acta Mater. 57 (2009) 5571-5581.

[14] M. Ohnuma, K. Hono, E. Abe, H. Onodera, S. Mitani, and H. Fujimori, J. Appl. Phys. 82 (1997) 5646-5652.

[15] I. Mirebeau, C. Bellouard, M. Hennion, H. L. Dormann, C. Djega-Mariadassou, and M. Tessier, J. Magn. Magn. Mater. 104-107 (1992) 1560-1562.

[16] D. H. Ping, M. Ohnuma, K. Hono, M. Watanabe, T. Iwasa, and T. Masumoto, J. Appl. Phys. 90 (2001) 4708-4716.

[17] X. Y. Xiong, M. Ohnuma, T. Ohkubo, D. H. Ping, K. Hono, S. Ohnuma, H. Fujimori, and T. Masumoto, J. Magn. Magn. Mater. 265 (2003) 83-93.

[18] S. Abe, M. Ohnuma, D. H. Ping, and S. Ohnuma, J. Appl. Phys. 104 (2008) 104305/1-4.

[19] Y. Oba, S. Koppoju, M. Ohnuma, T. Murakami, H. Hatano, K. Sasakawa, A. Kitahara, J. Suzuki, ISIJ Int. 51 (2011) 1852-1858.
[20] A. Wiedenmann, J. Appl. Cryst. 33 (2000) 428-432.
[21] J. Suzuki, K. Takei, Y. Maeda, and Y. Morii, J. Magn. Magn. Mater. 184 (1998) 116-125.
[22] S. J. Lister, M. P. Wismayer, V. Venkataramana, M. A. de Vries, S. J. Ray, S. L. Lee, T. Thomson, J. Kohlbrecher, H. Do, Y. Ikeda, K. Takano, and C. Dewhurst, J. Appl. Phys. 106 (2009) 063908/1-4.
[23] T. Oku, T. Kikuchi, T. Shinohara, J. Suzuki, Y. Ishii, M. Takeda, K. Kakurai, Y. Sasaki, M. Kishimoto, M. Yokoyama, Y. Nishihara, Physica B 404 (2009) 2575-2577.
[24] J. Löffler, H.-B. Braun, and W. Wagner, Phys. Rev. Lett. 85 (2000) 1990-1993.
[25] M. Furusaka T. Miyata, S. Takeda, Y. Oba, M. Ohnuma, S. Goko, N.L. Yamada, N. Torikai, F. Fujita, A. Homma, M. Sugiyama, T. Fujiwara, and H. Takahashi, KENS Rep. 17 (2011) 21-22.
[26] F. Zhang, J. Ilavsky, G. G. Long, J. P. G. Quintana, A. J. Allen, and P. R. Jemian, Metall. Mater. Trans. A 41 (2010) 1151-1158.
[27] J. S. Pedersen, Adv. Colloid Interface Sci. 70 (1997) 171-210.
[28] J. S. Pedersen, J. Appl. Cryst. 27 (1994) 595-608.
[29] V. B. Prokopenko, V. S. Gurin, A. A. Alexeenko, V. S. Kulikauskas, and D. L. Kovalenko, J. Phys. D: Appl. Phys. 33 (2000) 3152-3155.
[30] O. Yeshchenko, I. Dmitruk, A. Alexeenko, A. Dmytruk, and V. Tinkov, Physica E 41 (2008) 60-65.
[31] S. S. Mikhailova, O. V. Karban', O. A. Shilova, T. V. Khamova, and D. V. Surnin, Glass Phys. Chem 35 (2009) 479-483.
[32] X. Batlle and A. Labarta, J. Phys. D: Appl. Phys. 35 (2002) R15-R42.
[33] K. Osamura, H. Okuda, M. Takashima, K. Asano, and M. Furusaka, Mater. Trans. JIM 34 (1993) 305-311.
[34] M. Große, A. Gokhman, H. Böhmert, Nucl. Inst. Met. Phys Res. B 160 (2000) 515-520.
[35] M. J. Alinger, G. R. Odette, and D. T. Hoelzer, Acta Mater. 57 (2009) 392-406.
[36] B. S. Seong, E. Shin, S.-H. Choi, Y. Choi, Y. S. Han, K. H. Lee and Y. Tomota, Appl. Phys. A 99 (2010) 613-620.
[37] F. W. Constant, Phys. Rev. 36 (1930) 1654-1660.
[38] J. C. Ododo, J. Phys. F:Met. Phys. 13 (1983) 1291-1309.
[39] T. Shinohara, M. Shigemune, T. Sato, T. Taniyama and H. Sakurai, J. Phys. Soc. Jpn. 74 (2005) 1044-1048.

[40] R. L. Mozzi and B. E. Warren, J. Appl. Cryst. 2 (1969) 164-172.

[41] B. Hoex, F. J. J. Peeters, M. Creatore, M. A. Blauw, W. M. M. Kessels and M. C. M. van de Sanden, J. Vac. Sci. Technol. A 24 (2006) 1823-1830.

[42] W. L. Roth, J. Phys. Chem Solids 25 (1964) 1-10.

[43] F. J. Spooner and M. W. Vernon, J. Mater. Sci. 4 (1969) 734-742.

[44] N. Morimoto, M. Tokonami, M. Watanabe and K. Koto, Am. Mineral. 59 (1974) 475-485.

[45] F. Marumo, M. Isobe and S. Akimoto, Acta Cryst. B 33 (1977) 713-716.

[46] P. Villars, Pearson's handbook of Crystallographic Data for Intermetallic Phases, ASM International, Ohio, 1997.

[47] P. F. Carcia, A. D. Meinhaldt and A. Suna, Appl. Phys. Lett. 47 (1985) 178-180.

[48] S. Hashimoto, Y. Ochiai and K. Aso, Jpn. J. Appl. Phys. 28 (1989) 1596-1599.

[49] D. Weller, H. Brändle and C. Chappert, J. Magn. Magn. Mater 121 (1993) 461-470.

Table I Parameters D_A, D_B, σ_A and σ_B evaluated from the fitting.

Fig. 1 2D SAXS pattern of the $Co_{59}Pd_{11}Si_8O_{22}$ nanogranular film. The central dark spot is the shadow of a direct beam stop.

Fig. 2 Azimuthal plot of the SAXS intensity. The circle, diamond and triangle symbols are the intensities at 0.8-0.9, 1.5-1.6 and 3.0-3.1 nm^{-1}, respectively.

Fig. 3 q-dependent SAXS intensity. Open circles and solid line are experimental data and fitted curve, respectively. The line proportional to q^{-4} is also shown.

Fig. 4 q-dependent SANS intensities. The opaque triangle and open square plots are $I_{//}(q)$ and $I_{\perp}(q)$, respectively. While $I_{//}(q)$ is equal to the nuclear scattering $I_{nuc}(q)$, $I_{\perp}(q)$ includes both the magnetic and nuclear contributions. The broken line is the scaled $I_{SAXS}(q)$. The shape of $I_{\perp}(q)$ is almost the same as $I_{SAXS}(q)$ at high q.

Fig.5 Ratio of $I_{SAXS}(q)$ to $I_{\perp}(q)$. The horizontal dotted line indicates the average between q=1.2 and 2.5 nm^{-1}.

Fig. 6 Calculated values of $\Delta\rho_r^2$ for Co_xPd_{1-x} particles embedded in an SiO_2 matrix. The horizontal dotted line and the vertical dashed-dotted line indicate the experimental average of $I_{SAXS}/I_{\perp}$ and the chemical composition of the sample evaluated using RBS spectrometry, respectively.

Fig. 7 Magnetic hysteresis loops along with the magnetization easy (solid curve) and hard axes (broken curve).

Fig. 8 Calculated values of $\Delta\rho_r^2$ for Co_xPd_{1-x} particles embedded in CoO, α-Co_2SiO_4, β-Co_2SiO_4 and γ-Co_2SiO_4, matrices. The horizontal dotted line indicates the experimental average of $I_{SAXS}/I_{\perp}$.

Fig. 9 Calculated values of $\Delta\rho_r^2$ for $Co_{59-y}Pd_{11}$ particles embedded in $(CoO)_y(SiO_2)_8$. The horizontal dotted line indicates the experimental average of $I_{SAXS}/I_{\perp}$.

Table I

Particle	D_{ave} (nm)	σ (nm)
A	3.67±0.02	0.612±0.005
B	2.55±0.08	1.07±0.04

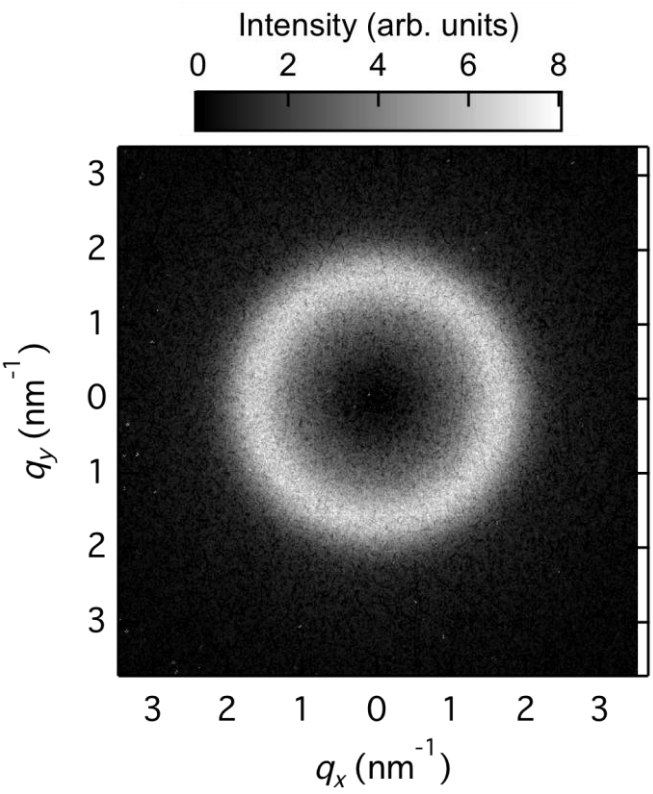
Intensity (arb. units)
0
2
4
6
8
3
2
1
0
1
2
3
q_y (nm^{-1})
3
2
1
0
1
2
3
q_x (nm^{-1})

Fig. 1

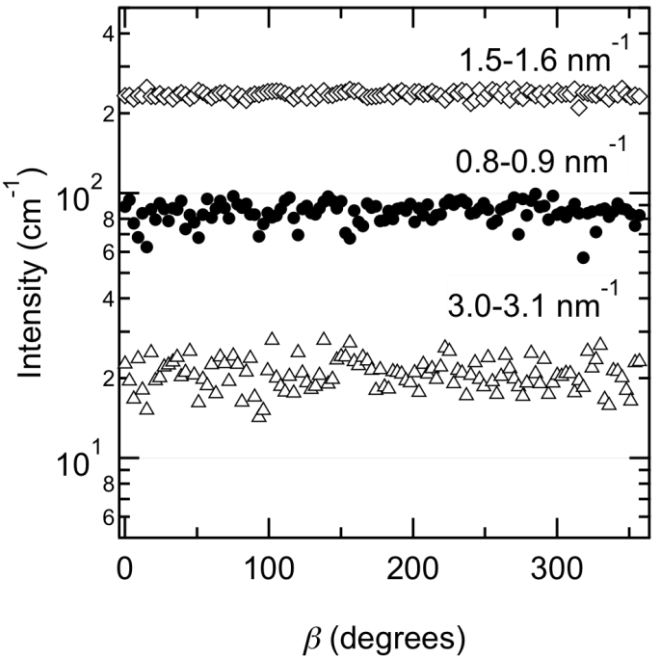
1.5-1.6 nm^{-1}
0.8-0.9 nm^{-1}
3.0-3.1 nm^{-1}
Intensity (cm^{-1})
10^2
10^1
0
100
200
300
β (degrees)

Fig. 2

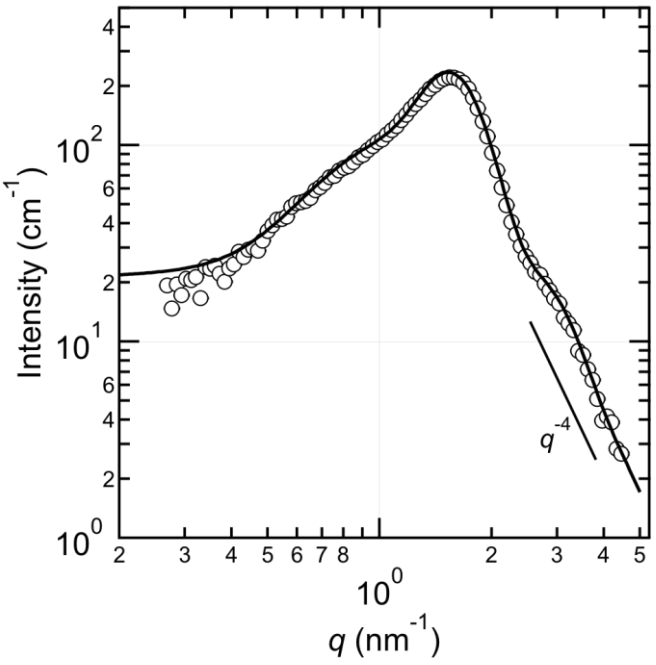
Intensity (cm^{-1})
q^{-4}
q (nm^{-1})

Fig. 3

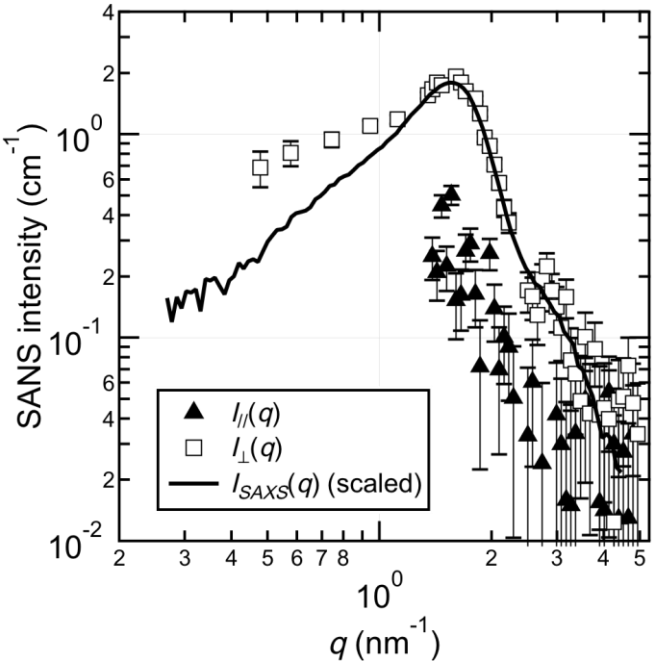
SANS intensity (cm^{-1})
$I_{//}(q)$
$I_{\perp}(q)$
$I_{SAXS}(q)$ (scaled)
q (nm^{-1})

Fig. 4

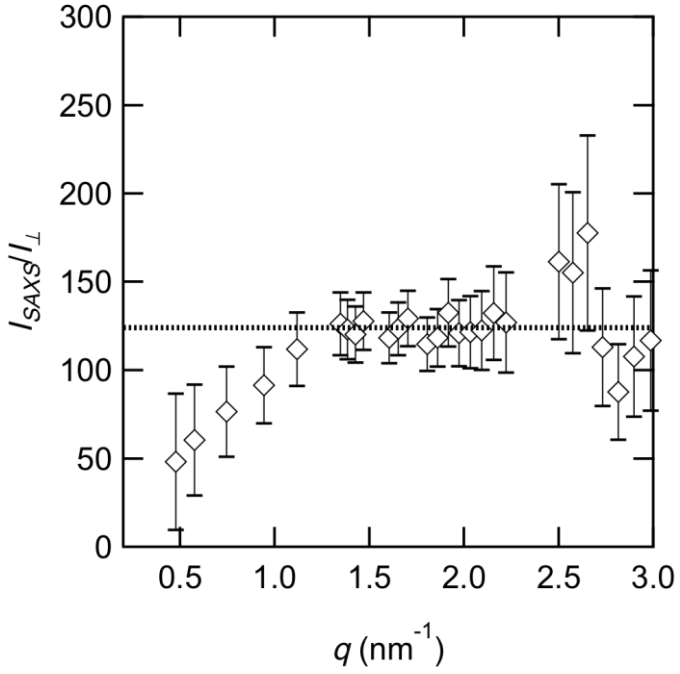
300
250
200
150
100
50
0
0.5
1.0
1.5
2.0
2.5
3.0
$I_{SAXS}/I_{\perp}$
q (nm^{-1})

Fig. 5

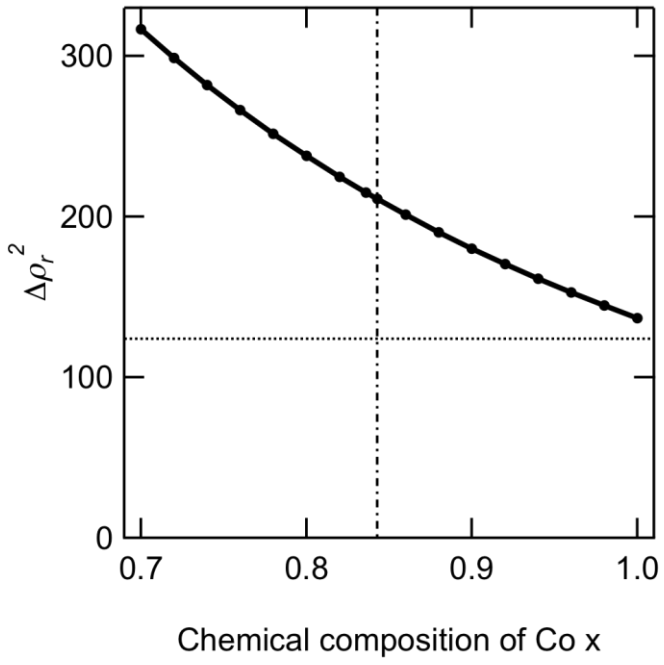
300
200
100
0
0.7
0.8
0.9
1.0
$\Delta\rho_r^2$
Chemical composition of Co x

Fig. 6

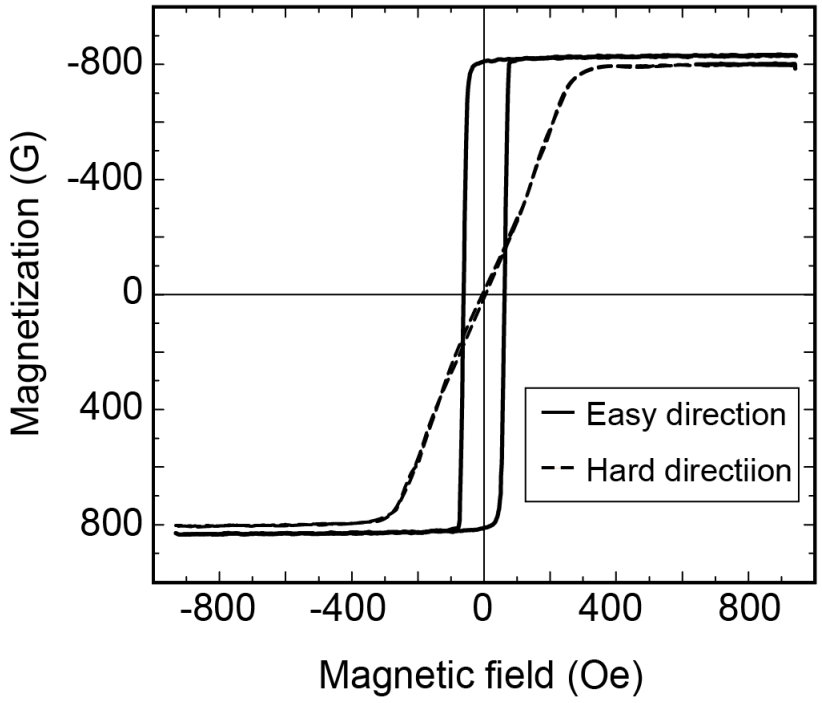
Magnetization (G)
-800
-400
0
400
800
-800
-400
0
400
800
Magnetic field (Oe)
Easy direction
Hard directiion

Fig. 7

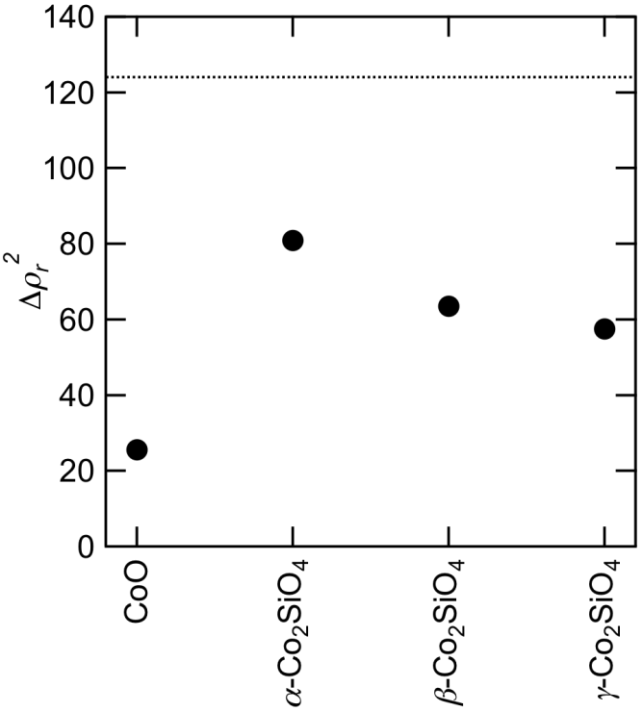
$\Delta\rho_r^2$
140
120
100
80
60
40
20
0
CoO
α-Co_2SiO_4
β-Co_2SiO_4
γ-Co_2SiO_4

Fig. 8

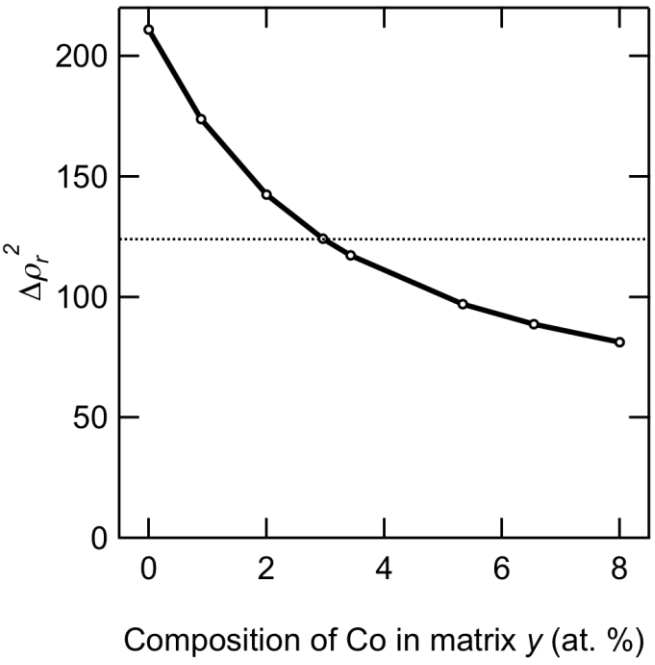
200
150
100
50
0
$\Delta\rho_r^2$
0
2
4
6
8
Composition of Co in matrix *y* (at. %)

Fig. 9